



ChemComm

**Electron Injection into Titanium Dioxide by Panchromatic
Dirhodium Photosensitizers with Low Energy Red Light**

Journal:	<i>ChemComm</i>
Manuscript ID	CC-COM-06-2019-004677.R2
Article Type:	Communication

SCHOLARONE™
Manuscripts

COMMUNICATION

Electron Injection into Titanium Dioxide by Panchromatic Dirhodium Photosensitizers with Low Energy Red Light

Congcong Xue,^a Hannah J. Sayre,^a and Claudia Turro*^a

Received 00th January 20xx,
Accepted 00th January 20xx

DOI: 10.1039/x0xx00000x

Two new Rh₂(II,II) dyes were synthesized and anchored to TiO₂ for charge injection upon irradiation. The ¹ML-LCT (metal/ligand-to-ligand charge transfer) excited state is populated upon excitation, which decays to the corresponding ³ML-LCT state. Ultrafast electron injection into TiO₂ from the Rh₂(II,II) dyes was achieved with low energy, red light excitation.

The increasing demand for energy urges the development of new sustainable, efficient, and clean energy sources.¹ Sunlight has been widely applied in the fields of dye sensitized solar cells (DSSCs) and dye-sensitized photoelectrochemical cells (DSPECs) to convert solar energy to electrical charge and to store energy in the form of chemical bonds.^{2–12} However, efficient collection of solar energy remains a challenge, in part because not all incident photons are absorbed by current photosensitizers, such that much of the sunlight remain unused.¹³ Although the solar spectrum that can potentially be used by sensitizers extends broadly from UV to the near-IR, traditional dyes do not substantially absorb low energy photons in the red and near-IR regions, which limits the potential incident photon to current efficiency (IPCE) of a given solar cell.

Thiocyanate-based Ru(II) polypyridyl complexes, such as the N3 dye, have been extensively investigated since their introduction in 1993 due to their relatively broad absorption range when compared to other Ru(II) photosensitizers with suitable redox properties.¹⁴ However, the lability of the Ru–SCN bonds over time and their limited ability to harvest near-IR photons reduce their overall performance.¹⁵ Porphyrin and phthalocyanines systems are known for their intense spectral response in the near-IR region, but they often suffer from unfavorable aggregation on the semiconductor surface.^{8, 16} Other organic dyes, such as coumarin and indoline, are cost-efficient alternatives to those containing ruthenium, but their narrow spectral response and difficult multi-step synthetic routes represent critical drawbacks to these systems.^{17, 18} As

such, a need remains for stable dye molecules with a broad absorption range and favorable redox properties for charge injection into n- or p-type semiconductors.

Previous work has demonstrated that Rh₂(II,II) formamidinate complexes, [Rh₂(DTolF)₂(L)₂][BF₄] (DTolF = *p*-ditolylformamidinate; L = bidentate chelating or bridging diimine ligand), feature a low energy transition that populates a state that results from the movement of electron density from the Rh₂(δ^{*})/formamidinate(π^{*}) highest occupied molecular orbital (HOMO) to a lowest unoccupied molecular orbital (LUMO) that is localized on a π^{*} MO of the diimine ligand.^{19–21} This singlet metal/ligand-to-ligand charge transfer (¹ML-LCT) excited state populated upon excitation undergoes intersystem crossing to generate the corresponding ³ML-LCT state.^{19, 20} Synthetic modification of Rh₂(II,II) complexes with ligands that are able to coordinate to the axial positions result in the extension of the ³ML-LCT lifetimes from ~500 ps to ~25 ns.²¹ Electron transfer reactions with methyl viologen and *p*-phenylenediamine have demonstrated that some Rh₂(II,II) complexes can perform bimolecular charge transfer, acting as both excited state reductants and oxidants. The broad absorption and excited state redox properties of Rh₂(II,II) complexes have already resulted in their application as photosensitizers for H₂ production upon 655 nm excitation.²² Herein, we present electron injection by **1** and **2** (Fig. 1) upon low energy irradiation, 600 nm for **1** and 520 nm for **2**, into anatase TiO₂ n-type semiconductor.

Complexes **1** and **2** were prepared according to synthetic procedures reported for the related complexes

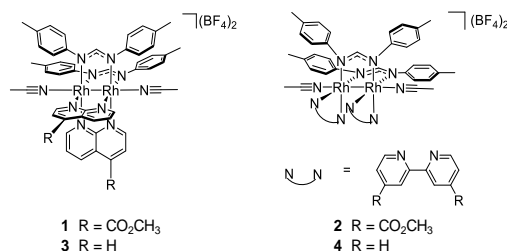


Fig. 1. Schematic representation of Rh₂(II,II) complexes **1** – **4**.

^a Department of Chemistry and Biochemistry, The Ohio State University, Columbus, OH 43210-1340, USA. Email: turro.1@osu.edu

Table 1. Electronic Absorption Maxima, Extinction Coefficients, and Reduction Potentials of **1** and **2** in CH₃CN.

Complex	$\lambda_{\text{abs}} / \text{nm}$ ($\epsilon / 10^3 \text{ M}^{-1} \text{ cm}^{-1}$)	$E_{1/2} / \text{V}^{\text{a}}$
1	271 (27.9), 306 (22.7), 450 (1.7), 630 (2.8)	+0.93, -0.61, -0.72, -1.33
2	241 (30.0), 312 (31.0), 387 (9.8), 595 (1.7)	+1.08, -0.28, -0.81, -1.16
3^b	300 (24.9), 436 (1.8), 566 (3.6)	+0.87, -0.94, -1.12 ^c
4	272 (28.3), 418 (2.3), 510 (0.6)	+0.86, -0.45, -1.20, -1.74

^a[Complex] = 0.5 mM, 0.1 M Bu₄NPF₆ in CH₃CN under N₂ atmosphere; vs Ag/AgCl. ^bElectronic absorption from ref. 25 and electrochemistry from ref. 21. ^cIrreversible.

[Rh₂(DTolF)₂(np)₂][BF₄]₂ (**3**; np = 1,8-naphthiridine)²⁰ and [Rh₂(DTolF)₂(bpy)₂][BF₄]₂ (**4**; bpy = 2,2'-bipyridine),²³ described in detail in the Electronic Supporting Information (ESI). The bridging np ligands shorten the Rh-Rh bond length to 2.4466(7) Å in **3**, as compared to 2.5821(5) Å in **4**, which contains chelating bpy ligands.^{23, 24} The shorter Rh-Rh bond length in **3** results in a destabilized Rh₂(σ*) MO relative to that in **4**, composed of the antibonding linear combination of the d_{z²} orbitals on each metal and, consequently, on a higher energy metal centered (³MC) state.²⁴ Based on comparisons with structurally related Rh₂(II,II) complexes, it is expected that the Rh-Rh bond length of **1** will be similar to that for **3**, and that for **2** close to the Rh-Rh distance reported for **4**.^{19, 25} The steady-state electronic absorption spectra of **1** and **2** in CH₃CN are shown in Fig. S3 and summarized in Table 1. A broad, low-energy absorption band with maximum at 595 nm ($\epsilon = 1,700 \text{ M}^{-1} \text{ cm}^{-1}$) is observed for **2**, which shifts to a lower energy in **1**, 630 nm ($\epsilon = 2,800 \text{ M}^{-1} \text{ cm}^{-1}$). These transitions are consistent with those of previously reported complexes, such as **3** with $\lambda_{\text{abs}} = 566 \text{ nm}$ ($\epsilon = 3600 \text{ M}^{-1} \text{ cm}^{-1}$) and [Rh₂(DTolF)₂(dpq)₂][BF₄]₂ (dpq = dipyrido[3,2-f:2',3'-h]quinoxaline) with $\lambda_{\text{abs}} = 525 \text{ nm}$ ($\epsilon = 1300 \text{ M}^{-1} \text{ cm}^{-1}$). Based on these comparisons, these bands are assigned as ¹ML-LCT in nature arising from a Rh₂(δ*)/DTolF(π*) → menp(π*) transition in **1** and Rh₂(δ*)/DTolF(π*) → dmeb(π*) in **2**.

The half-wave potentials measured for **1** and **2** in CH₃CN and are listed in Table 1. Complexes **1** and **2** exhibit a reversible one-electron oxidation corresponding to Rh₂^{III,II/II,II} couples at +0.93 V and +1.08 V vs Ag/AgCl, respectively, which compare well to those measured for **3** at +0.87 V and **4** at +0.86 V vs Ag/AgCl in the same solvent (Table 1). The first and second cathodic couples of **1** are assigned to the sequential reduction on the two menp ligands and are observed at -0.61 V and -0.72 V vs Ag/AgCl. These values compare well to those reported for the reduction of the np ligands in **3** at -0.81 V and -1.16 V vs Ag/AgCl.²⁰ The anodic shifts observed of the reduction of menp ligands in **1** as compared to the np ligands in **3** is attributed to the electron withdrawing methyl ester group on the menp ligand. For **2**, the first cathodic couple at -0.28 V is assigned to the one-electron reduction of the bimetallic core, Rh₂^{III,II/II,II}. The reduction of one dmeb ligand is observed in **2** at -0.81 V, followed by another reversible couple at -1.16 V vs Ag/AgCl in CH₃CN (Table 1). As in the case of menp and np, the anodic shift of the ligand-based reduction of dmeb in **2** relative to that of bpy in **4** arises from the presence of the electron donating methyl ester substituent.

The photophysical properties of **1** and **2** were examined in CH₃CN and compared to those of the corresponding parent complexes **3** and **4**, respectively. The femtosecond time-resolved infrared spectra (fsTRIR) of **1** following 600 nm excitation (IRF = 85 ps) shown in Fig. 2a exhibits two ground state bleach features at 1512 cm⁻¹ and 1574 cm⁻¹ corresponding to two asymmetric ν(N=C-N) stretches of the DTolF ligand, as previously reported for the related complex **1** at 1507 cm⁻¹ and 1577 cm⁻¹.²⁰ One ν(C=O) stretch bleach at 1732 cm⁻¹ associated with the methyl ester functional group of **1** is also observed, consistent with the ground state IR stretch of the complex and that of the free menp ligand at 1729 cm⁻¹. The excited state ν(N=C-N) vibrations shift to 1536 cm⁻¹ and 1600 cm⁻¹, and the ν(C=O) stretch is observed at 1673 cm⁻¹ in the excited state. The shift of the DTolF vibrations to higher energy and ester vibration to lower energy in the excited state arise from the movement of electron density from the Rh₂(δ*)/DTolF(π*) HOMO to the menp(π*) LUMO, which confirms the assignment of a ML-LCT excited state in this complex. The lifetime of the positive signals can be fitted to a biexponential function with lifetimes of 2.6 ps and 429 ps associated with the ¹ML-LCT and ³ML-LCT excited states, respectively. Similar excited state features were reported for **3** with ¹ML-LCT and ³ML-LCT lifetimes of 16 ps and 424 ps.²⁰

Similar results were observed with **2**, where the fsTRIR spectra exhibit three asymmetric ν(N=C-N) ground state bleaches at 1520 cm⁻¹, 1580 cm⁻¹ and 1620 cm⁻¹, and one ν(C=O) bleach at 1740 cm⁻¹ (Fig. 2b). The lack of the positive excited state absorption signal associated with the ν(N=C-N) bleaches could be due to a smaller extent of charge transfer excited state resulting from enhanced mixing with the lower-energy MC state in **2** as compared to **1**, attributed to the longer Rh-Rh bond in the former. The excited state ν(C=O) stretch of **2** is observed at 1720 cm⁻¹. The smaller C=O shift in **2**, Δν = -20 cm⁻¹, as compared to that in **1**, Δν = -60 cm⁻¹, is attributed to the presence of two symmetric methyl ester groups on the dmeb ligand relative to only one on menp. It is expected that there is a higher degree of polarization in the ML-LCT excited state of **1** because the electron density will be localized asymmetrically on one side of the ligand. Similar effects on the magnitudes of Δν(C=O) shifts in the excited states were

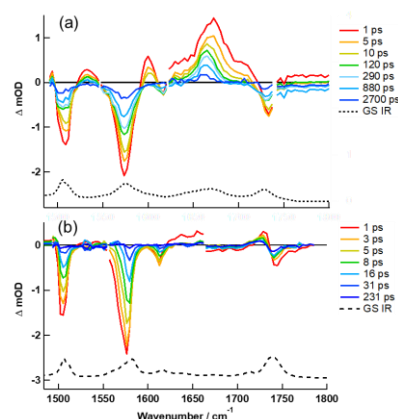


Fig. 2 fsTRIR spectra of (a) **1** and (b) **2** in CD₃CN $\lambda_{\text{exc}} = 600 \text{ nm}$, 2 μJ) and corresponding ground state IR spectra (dashed lines).

previously reported for ruthenium polypyridyl complexes. $[\text{Ru}(\text{bpy})_2(4,4'-(\text{CO}_2\text{Et})_2\text{bpy})]^{2+}$, with a bpy ligand substituted in a symmetric fashion, exhibits a less pronounced shift as compared to the asymmetric substituted complex, $[\text{Ru}(\text{bpy})_2(4-\text{CO}_2\text{Et}-4'-\text{CH}_3\text{bpy})]^{2+}$.²⁶

The femtosecond transient absorption (fsTA) spectra of **1** and **2** are characterized by broad excited state absorption in the visible region, as shown in Fig. S4, observed from 400 to 540 nm for **1** with peaks at 435 and 510 nm. The lower intensity in the 450–500 nm range is attributed to the superimposed ground state bleach signal with absorption maximum at 450 nm. The decay of the signal at 440 nm was fitted to a biexponential function with $\tau_1 = 4$ ps (43%) and $\tau_2 = 460$ ps (57%). The fsTA previously reported for **3** also shows broad absorption from 350 to 550 nm with peaks at ~ 400 and ~ 500 nm, consistent with the spectral features of the one-electron reduced and one-electron oxidized complex recorded in spectroelectrochemistry experiments.²⁰ These results are consistent with the fsTRIR data, where the short and long components are assigned to ¹ML-LCT and ³ML-LCT excited states, respectively.

As shown in Fig. S4b, the fsTA spectra of **2** features a broad absorption band from 450 to 650 nm with an apparent maximum at ~ 640 nm in CH_3CN ($\lambda_{\text{exc}} = 520$ nm, IRF = 85 fs). The decay at 640 nm is fitted biexponentially to 2.5 ps and 56 ps. The spectroelectrochemistry of **2** collected at an applied potential, E_{app} , of +1.37 V vs Ag/AgCl, expected to result in the formation of the one-electron oxidized $\text{Rh}_2(\text{III},\text{II})$ complex, exhibits minimal spectral changes (Fig. S5). In contrast, reduced **2**, recorded at $E_{\text{app}} = -0.57$ V corresponding to the $\text{Rh}_2(\text{II},\text{I})$ complex, possesses characteristic peaks at 470 and 570 nm that are not observed in the fsTA (Fig. S4b). The observed broad absorption at $\lambda > 500$ nm is consistent with $\pi\pi^*$ transitions of the reduced dmb ligand, as previously reported for complexes related one-electron reduced ligands.^{27–29}

It is important to note that the electrochemistry of **2** points at a LUMO localized on the dirhodium core, resulting in a spectrum of the ground state one-electron reduced complex associated with the $\text{Rh}_2(\text{II},\text{I})$ complex. However, the fsTA spectrum is not consistent with the spectroelectrochemistry, and instead resembles the reduced dmb ligand. Together with the electron density shift observed in the fsTRIR of **2**, the results point at singlet and triplet excited states that are ML-LCT in character. In the case of **1**, the first reduction is attributed to placement of an electron on the menp ligand, since the bridging nature of the substituted np ligand raises the energy of the $\text{Rh}_2(\sigma^*)$ MO, such that it is orbital is not the LUMO.

The electron transfer from excited Ru(II) dyes to TiO_2 has been shown to take place from both the ¹MLCT and ³MLCT states, although the singlet state is short-lived, < 50 fs, such that extended lifetimes are not necessary for a dye to inject electrons into n-type semiconductors.^{17,30} Given the longer ¹ML-LCT lifetimes of **1** and **2** as compared to Ru(II) sensitizers, it is expected that these states would undergo charge injection. To this end, the singlet excited states oxidation potentials, ${}^1E_{\text{ox}}$, of **1** and **2** were estimated to determine the driving force for electron injection to TiO_2 and the modified Latimer diagrams for **1** and **2** are shown in Fig. S6. The energy of the ¹ML-LCT state,

E_{00} , for **1** is estimated to be ~ 1.7 eV from the tail of its electronic absorption spectrum, resulting in ${}^1E_{\text{ox}} \sim -0.8$ V vs Ag/AgCl, and a similar calculation resulted in ${}^1E_{\text{ox}} \sim -0.7$ V vs Ag/AgCl for **2**. The higher ${}^1E_{\text{ox}}$ value compared to the lower limit of the TiO_2 conduction band ($E_{\text{CB}} \sim -0.4$ eV vs Ag/AgCl)³¹ makes electron injection thermodynamically favorable for both complexes. However, electron injection from the triplet excited state is unfavorable, with calculated ${}^3E_{\text{ox}}$ values of approximately -0.2 V and -0.1 V vs Ag/AgCl for **1** and **2**, respectively.

The electron injection into TiO_2 sensitized by **1** was measured by fsTRIR. Unlike fsTA, fsTRIR (in mid-IR region) will directly probe the electron absorption within the semiconductor without the superposition of the excited state or oxidized dye signal.^{32–34} Complex **1** was anchored to the surface of TiO_2 and purified as described in the ESI, and the resulting **1**@ TiO_2 nanoparticles were suspended in CD_3CN for the spectroscopic studies. Unlike the fsTRIR spectra collected for **1** (Fig. 2a), the spectra of **1**@ TiO_2 show broad positive signal in the mid-IR region attributed to the free moving electrons injected from the ¹ML-LCT excited state of **1** into the conduction band (CB) of TiO_2 (Fig. 3).³⁵ Superimposed on this broad absorption, a weak bleach at ~ 1570 cm^{-1} is observed assigned to the $\nu(\text{N}=\text{C}=\text{N})$ stretch of the anchored dye. In the absence of sensitizer, no broad electron signal was observed for TiO_2 under the similar experimental conditions. As expected from the absence of anchoring groups on the np ligand, excitation of **3** and TiO_2 did not result in charge injection, although the same sample preparation procedure was followed as in the case of **1**.

The ultrafast increase of the mid-IR absorption upon excitation with a risetime within the instrument response time of ~ 130 fs is consistent with electron injection from the vibrationally hot ¹ML-LCT excited state of **1** to TiO_2 (Fig. S8a). The mid-IR signal measured at 1610 cm^{-1} decays with $\tau_1 = 9$ ps and $\tau_2 = 243$ ps, but the signal persists beyond the range of the experiment ($\tau_3 \gg 3$ ns). Bi- and triphasic charge recombination kinetics, resulting in a decrease of the mid-IR signal, have been generally observed for dye- TiO_2 systems with decays that typically range from hundreds of ps to ms.^{35–37} Thus, the longer components τ_2 and τ_3 are assigned to charge recombination. The $\tau_1 = 9$ ps component is faster than is typically observed and may be due to geminate charge recombination to the ground or the triple state of the dye. In addition, it has been previously reported that “hot” electrons injected from energies above the CB edge can relax down to the CB edge, also resulting in a decrease in the IR absorption cross-section and reduced signal arising from the reduced density of states, as previously observed for Ru(II) and Re(I) complexes,³⁷ as well as a Mo_2

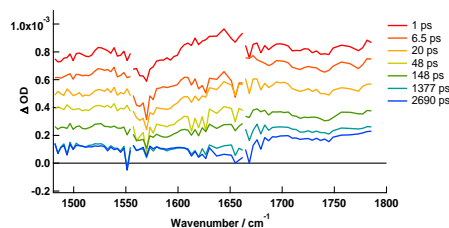


Fig. 3 fsTRIR spectra of **1**@ TiO_2 in CD_3CN (2 mJ, $\lambda_{\text{exc}} = 600$ nm)

paddlewheel complex.³⁶ Herein, the 600 nm excitation of **1** results in ultrafast electron injection from the hot ¹ML-LCT state, placing the electron ~0.8 V above the TiO₂ CB. Therefore, the short component may be ascribed to back electron transfer or to "hot" electron cooling within TiO₂. Similar results are observed for **2**@TiO₂ upon 520 nm excitation (Fig. S9). The electron injection efficiencies for **1** and **2** are calculated to be 97% and 95%, respectively (ESI).

In conclusion, this work represents of the first example of charge injection into a semiconductor, TiO₂ nanoparticles, by a Rh₂ photosensitizer. Both **1** and **2** process ¹ML-LCT excited states with picosecond lifetimes that decay to generate the corresponding ³ML-LCT excited state. The geometry of the complexes creates charge separated excited states in which holes are localized on Rh₂(δ*)/DTolF(π*) HOMO and electrons are on the menp(π*) or dmeb(π*) LUMOs. From the excited state reduction potentials, it can be predicted that charge injection from the ¹ML-LCT states of **1** and **2** into TiO₂ is thermodynamically favorable, but not from their ³ML-LCT states, consistent with absence of a slower component. The panchromatic dirhodium complexes represent a new family of photosensitizers able to harvest more lower energy photons than traditional dyes to make better use of the solar spectrum. The synthetic modification of the bridging or chelating ligands can be used to tune the energetics of the excited states to further develop this class of near-IR light absorbing dyes.

The authors thank National Science Foundation (CHE-1800395) and The Ohio State University for partial support of this work, as well as the use of the Center for Chemical and Biophysical Dynamics at OSU to conduct all the femtosecond spectroscopy experiments and Dr. Barbara Dunlap for her help.

Conflicts of interest

There are no conflicts to declare.

Notes and references

1. T. W. Brown, T. Bischof-Niemz, K. Blok, C. Breyer, H. Lund and B. V. Mathiesen, *Renew. Sust. Energ. Rev.*, 2018, **92**, 834-847.
2. A. Hagfeldt, G. Boschloo, L. Sun, L. Kloo and H. Pettersson, *Chem. Rev.*, 2010, **110**, 6595-6663.
3. M. Freitag, J. Teuscher, Y. Saygili, X. Zhang, F. Giordano, P. Liska, J. Hua, S. M. Zakeeruddin, J.-E. Moser, M. Grätzel and A. Hagfeldt, *Nat. Photonics*, 2017, **11**, 372.
4. M. K. Nazeeruddin, E. Baranoff and M. Grätzel, *Sol. Energy*, 2011, **85**, 1172-1178.
5. J. Li and N. Wu, *Catal. Sci. Technol.*, 2015, **5**, 1360-1384.
6. D. Wang, B. D. Sherman, B. H. Farnum, M. V. Sheridan, S. L. Marquard, M. S. Eberhart, C. J. Dares and T. J. Meyer, *Proc. Natl. Acad. Sci.*, 2017, **114**, 9809.
7. P. Xu, C. L. Gray, L. Xiao and T. E. Mallouk, *J. Am. Chem. Soc.*, 2018, **140**, 11647-11654.
8. M. Urbani, M.-E. Ragoussi, M. K. Nazeeruddin and T. Torres, *Coord. Chem. Rev.*, 2019, **381**, 1-64.
9. D. Wang, S. L. Marquard, L. Troian-Gautier, M. V. Sheridan, B. D. Sherman, Y. Wang, M. S. Eberhart, B. H. Farnum, C. J. Dares and T. J. Meyer, *J. Am. Chem. Soc.*, 2018, **140**, 719-726.
10. M. K. Brennaman, R. J. Dillon, L. Alibabaei, M. K. Gish, C. J. Dares, D. L. Ashford, R. L. House, G. J. Meyer, J. M. Papanikolas and T. J. Meyer, *J. Am. Chem. Soc.*, 2016, **138**, 13085-13102.
11. I. Purnama, Salmahaminati, M. Abe, M. Hada, Y. Kubo and J. Y. Mulyana, *Dalton Trans.*, 2019, **48**, 688-695.
12. J. Sun, Y. Yu, A. E. Curtze, X. Liang and Y. Wu, *Chem. Sci.*, 2019, **10**, 5519-5527.
13. S. Mozaffari, M. R. Nateghi and M. B. Zarandi, *Renew. Sust. Energ. Rev.*, 2017, **71**, 675-686.
14. M. K. Nazeeruddin, A. Kay, I. Rodicio, R. Humphry-Baker, E. Mueller, P. Liska, N. Vlachopoulos and M. Graetzel, *J. Am. Chem. Soc.*, 1993, **115**, 6382-6390.
15. G. C. Vougioukalakis, A. I. Philippopoulos, T. Stergiopoulos and P. Falaras, *Coord. Chem. Rev.*, 2011, **255**, 2602-2621.
16. M.-E. Ragoussi, M. Ince and T. Torres, *Eur. J. Org. Chem.*, 2013, **2013**, 6475-6489.
17. K. Hara, Z.-S. Wang, T. Sato, A. Furube, R. Katoh, H. Sugihara, Y. Dan-oh, C. Kasada, A. Shinpo and S. Suga, *J. Phys. Chem. B*, 2005, **109**, 15476-15482.
18. S. Ito, H. Miura, S. Uchida, M. Takata, K. Sumioka, P. Liska, P. Comte, P. Péchy and M. Grätzel, *Chem. Commun.*, 2008, 5194-5196.
19. Z. Li, N. A. Leed, N. M. Dickson-Karn, K. R. Dunbar and C. Turro, *Chem. Sci.*, 2014, **5**, 727-737.
20. T. J. Whittemore, H. J. Sayre, C. Xue, T. A. White, J. C. Gallucci and C. Turro, *J. Am. Chem. Soc.*, 2017, **139**, 14724-14732.
21. T. J. Whittemore, A. Millet, H. J. Sayre, C. Xue, B. S. Dolinar, E. G. White, K. R. Dunbar and C. Turro, *J. Am. Chem. Soc.*, 2018, **140**, 5161-5170.
22. H. J. Sayre, A. Millet, K. R. Dunbar and C. Turro, *Chem. Commun.*, 2018, **54**, 8332-8334.
23. H. T. Chifotides, K. V. Catalan and K. R. Dunbar, *Inorg. Chem.*, 2003, **42**, 8739-8747.
24. T. A. White, K. R. Dunbar, R. P. Thummel and C. Turro, *Polyhedron*, 2016, **103**, 172-177.
25. H. T. Chifotides, B. Saha, N. J. Patmore, K. R. Dunbar and J. K. Bera, *Group 9 Metal-Metal Bonds*, 2015.
26. K. M. Omberg, G. D. Smith, D. A. Kavaliunas, P. Chen, J. A. Treadway, J. R. Schoonover, R. A. Palmer and T. J. Meyer, *Inorg. Chem.*, 1999, **38**, 951-956.
27. C. M. Elliott and E. J. Hershenhart, *J. Am. Chem. Soc.*, 1982, **104**, 7519-7526.
28. G. A. Heath, L. J. Yellowlees and P. S. Braterman, *J. Chem. Soc., Chem. Commun.*, 1981, 287-289.
29. D. M. Peloquin, D. R. Dewitt, S. S. Patel, J. W. Merkert, B. T. Donovan-Merkert and T. A. Schmedake, *Dalton Trans.*, 2015, **44**, 18723-18726.
30. A. Listorti, B. O'Regan and J. R. Durrant, *Chem. Mater.*, 2011, **23**, 3381-3399.
31. Y. Xu and M. A. A. Schoonen, *Am. Mineral.*, 2000, **85**, 543-556.
32. J. Sá, P. Friedli, R. Geiger, P. Lerch, M. H. Rittmann-Frank, C. J. Milne, J. Szlachetko, F. G. Santomauro, J. A. van Bokhoven, M. Chergui, M. J. Rossi and H. Sigg, *Analyst*, 2013, **138**, 1966-1970.
33. M. Abdellah, A. M. El-Zohry, L. J. Antila, C. D. Windle, E. Reisner and L. Hammarström, *J. Am. Chem. Soc.*, 2017, **139**, 1226-1232.
34. M. Juozapavicius, M. Kaucikas, J. J. van Thor and B. C. O'Regan, *J. Phys. Chem. C*, 2013, **117**, 116-123.
35. N. A. Anderson and T. Lian, *Annu. Rev. Phys. Chem.*, 2004, **56**, 491-519.
36. S. E. Brown-Xu, M. H. Chisholm, C. B. Durr, T. L. Gustafson and T. F. Spilker, *J. Am. Chem. Soc.*, 2014, **136**, 11428-11435.
37. J. B. Asbury, N. A. Anderson, E. Hao, X. Ai and T. Lian, *J. Phys. Chem. B*, 2003, **107**, 7376-7386.